JOURNAL OF MATERIALS SCIENCE **40** (2005) 2287–2293

Effects of roughness pitch of surfaces on their wettability

H. NAKAE, M. YOSHIDA, M. YOKOTA*
Waseda University, Tokyo, Japan

The surface roughness factors, such as the Wenzel roughness factor and so on, are very interrelated to each other. Therefore, it makes a precise discussion difficult on how the surface roughness affects the wettability. We already reported the effect of the surface roughness on the wettability at a constant Wenzel roughness factor using two kinds of models, the hemisphere close packing model and the hemiround rod close lining model. Nevertheless, the pitch is proportional to the height in these models. Therefore, we could not independently discuss the influence of roughness height and roughness pitch on the wettability.

We developed our new models which can independently describe the influence of the surface roughness height and the roughness pitch on the wettability. We simulated loose packing sphere models by periodically placing small ball bearings and the loose lining round rod models by winding fine wires. The wettability was measured by the sessile drop method for the non-wetting system using paraffin coated samples and aqueous solutions. These results show that there is a critical pitch which determines the maximum contact angle in both systems. These results can be explained by the ratio of the solid/liquid/vapor and liquid/vapor line length at the three phase line.

1. Introduction

It is well known that the surface roughness of a solid significantly affects its wettability [1–6]. The influence of the surface roughness on the wettability has been investigated by many researchers using surface roughness factors such as the Wenzel roughness factor [1], the Cassie equation [2, 3, 7–9], etc. For changing the roughness of a solid surface, many researchers used powders [10], photoresist micropatterns [11, 12], a porous surface [4, 10], a spherical stylus surface [13] and a regular pyramid surface [14]. However, their roughness factors depended on each other which make a precise discussion difficult. We already reported the effect of surface roughness on the wettability at a constant Wenzel roughness factor using two kinds of models, namely, the hemispheres close packing model and the hemiround rod close lining mode [7]. By using these models, the roughness height can be varied based on the radii of the spheres and rods. This means that the Wenzel roughness factors, calculated on the basis of the diameter in both models, are constant. Therefore, the effect of the surface roughness height on the wettability can then be discussed without changing the Wenzel roughness factors.

Nevertheless, we could not independently change the roughness height and the roughness pitch in these models. Therefore, we developed our new models which can be used to separately discuss the influence of the roughness height and the roughness pitch on the wettability. We made two kinds of surface models, namely the loose packing sphere models and the loose lining round rod models.

2. Experimental concept and procedure

The loose lining round rod (LLRR) models were made using a lathe by winding fine stainless wires around a half machined brass bar on the longitudinal surface. Fig. 1 shows photos of these samples. The roughness height h_r, namely the diameter of the wire, was 50 μm and the spacings, λ, were 50 μm (close lining), 100 and 200 μm, observed by a long-distance optical microscope. As can be clearly seen, the spacing is perfectly constant.

The loose packing sphere (LPS) models were made by placing small steel ball bearings on a sieve with the spacing of λ and transferring them on a glass plate. The SEM photograph of the LPS model is shown in Fig. 2 as an oblique view. The diameter of the balls, the roughness height h_r, was 200 μm and the spacing, λ, was 254 μm. These rough surface models were then coated with few microns thick paraffin layer using an ether solution [7].

The sessile drop method was used for the measurement of the contact angle in the non-wetting system with the paraffin-coated samples and aqueous solutions.

Present address: Nissan Motor Co. Ltd., Yokohama, Japan.

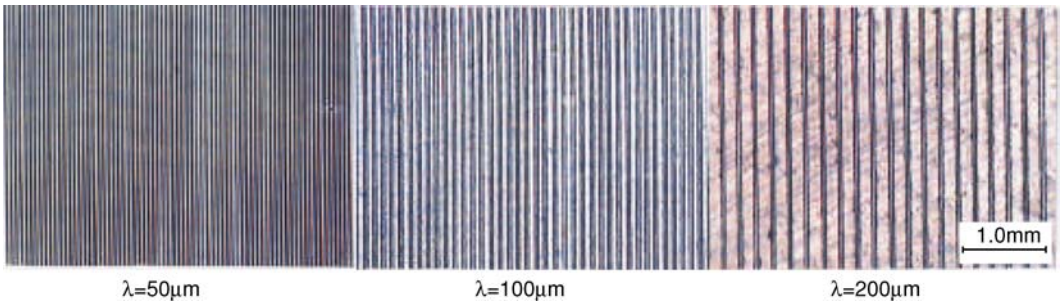

Figure 1 Photographs of LLRR surfaces ($h_r = 50\ \mu$m): (a) $\lambda = 50\ \mu$m, (b) $\lambda = 100\ \mu$m and (c) $\lambda = 200\ \mu$m.

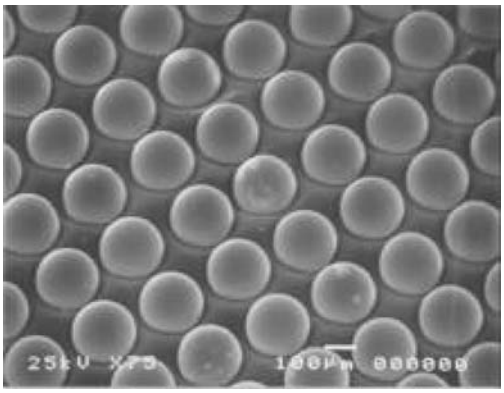

Figure 2 Oblique view of SEM photograph for LPS surface ($h_r = 200\ \mu$m, $\lambda = 254\ \mu$m).

In these experiments, we used pure water and the aqueous solution containing 0.05 mass% of a surfactant, sodium n-dodecyl sulfate (SDS). The volume of a sessile drop was about 4 mm^3. The contact angle between paraffin and pure water is 107°, which is nearly identical to the value reported by Asahara [15] and Navascues [16], and that of paraffin and aqueous solution is 96°.

The experimental conditions are summarized in Table I. In this table, the roughness height, h_r, is equal to the diameter of the spheres and the rods. The roughness pitch, λ, can be freely changed as shown in the table.

The aspect ratio of surface, A_r, and the Wenzel roughness factor, r_w, were defined by Kawai *et al*. [12] using the rough surface formed by photolithography as following,

$$A_r = \text{Pattern height}/\text{Bottom space} = h_r/(\lambda - h_r) \quad (1)$$

$$r_w = 1 + 2A_r \quad (2)$$

In the case of the hemisphere close packing model, the roughness factor, r_w, is nearly equal to 1.9 and that of the r_w for the hemiround rod close lining models is nearly equal to 1.6 and they are independent of their radii [7]. Nevertheless, the Wenzel roughness factors of the loose models are changed by h_r and λ as shown by the following equation.

$$r_w = 1 + 2A_r = 1 + 2h_r/(\lambda - h_r) \quad (3)$$

The experimental parameters and factors in each surface model are shown in Table II. The influence of r_w, h_r and A_r on the wettability can be discussed using these two new models.

For the measurement of the contact angle between the rough surface samples and the aqueous solutions, we used an automatic measurement system equipped with a CCD camera [7]. The apparent contact angle (hereafter, we used simply the contact angle), ϕ, was calculated using a microcomputer based on the height of the liquid drop, h, and the base line radius, r_b, of the liquid drop on the TV monitor. The calculation method for ϕ is based on a spherical cap model as follows,

$$\phi = 2\tan^{-1}(h/r_b) \quad (4)$$

The measurement was repeated 30 to 50 times for one system using different liquid drops. As for the contact angle, the mean value of the contact angles was adopted and the scatter band was shown by twice the standard deviation. Nevertheless, we observed the contact angle of the liquid drops on the LLRR surface from two directions, namely, the parallel direction and the normal direction to the rods due to the anisotropy of this solid surface.

TABLE I Experimental conditions for rough surfaces

Model		Size (μm)	
LLRR	h_r	50	100
	λ	50, 75, 100, 125, 150, 200, 250	100, 120, 150, 180, 200, 250, 300, 400, 500
LPS	h_r	200	300
	λ	200, 254, 330, 360, 508	300, 359, 423, 508, 598

LLRR model: Loose lining round rod model.
LPS model: Loose packing sphere model.

TABLE II Experimental parameters and factors in each surface model

Model	Parameters	r_w	h_r	A_r
Powder [10]	Powder size	V	V	V
Photoresist [11, 12]	h_r, λ	V	V	V
Pyramid [14]	h_r, λ	C	V	C
HSCPM[a] [7]	h_r	C(1.9)	V	C(∞)
HRRCLM[b] [7]	h_r	C(1.6)	V	C(∞)
LLRR	h_r, λ	V	V	V
LPS	h_r, λ	V	V	V

[a]HSCPM: Hemispheres close packing model.
[b]HRRCLM: Hemiround rod close lining model.

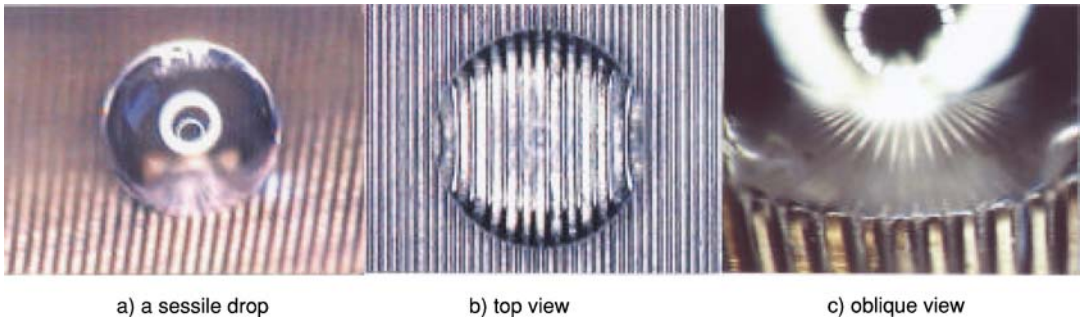

Figure 3 Over views of a liquid drop on LLRR surface ($h_r = 50\ \mu$m, $\lambda = 150\ \mu$m): (a) Top view, (b) Oblique view and (c) High magnification of b).

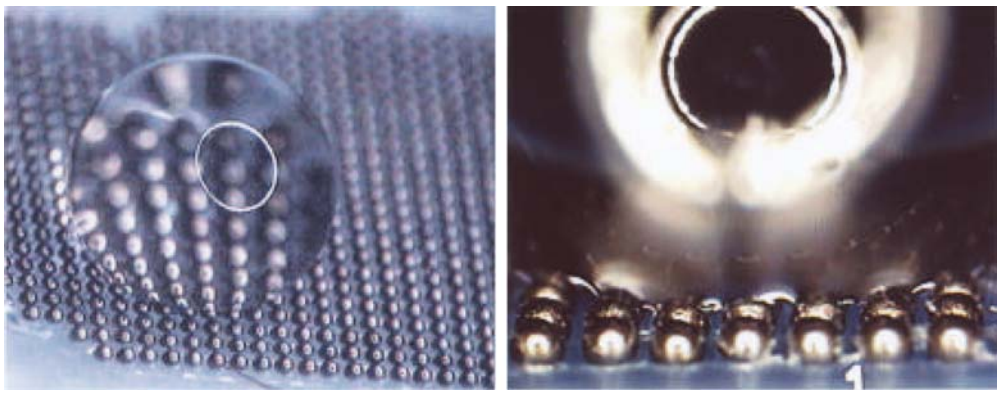

Figure 4 Top view and side view of a liquid drop on LPS surface. ($h_r = 200\ \mu$m and $\lambda = 254\ \mu$m).

3. Experimental results

3.1. Rough surface models and shape of the liquid drop

Fig. 3 shows the overview photographs of a liquid drop on the LLRR surface, where $h_r = 100\ \mu$m and $\lambda = 200\ \mu$m, observed from the oblique (a) and the top (b) using a stereoscopic optical long-distance microscope. As can be clearly seen, the shape of the liquid drop observed from the top is nearly spherical despite of the anisotropy of the solid sample. The solid/liquid/vapor (abbreviated *S/L/V*) interface observed from the oblique side is shown in Fig. 3c), a high magnification photograph. We can clearly see the three phase line of the *S/L/V* interface in this photograph. As can be clearly seen, the line consists of the *S/L/V*, *S/L* and liquid/vapor (abbreviated *L/V*) interface which means that part of the liquid phase detaches from the substrate.

Fig. 4 shows the low (a) and high (b) magnification oblique view photographs of a liquid drop on the LPS surface in which $h_r = 200\ \mu$m and $\lambda = 254\ \mu$m, observed with the optical microscope. We can recognize the size difference between the liquid drop and the ball with the low magnification photo and the *S/L/V* line from the high magnification photo. shape of the *L/V* interface is concave due to the intrinsic contact angle and the contact angle between the *L/V* that should be 180°. If the λ is larger than 254 μm, the shape changes from concave to convex. The details will be discussed later.

As it can be clearly seen from Fig. 4b, the high magnification image, we can confirm that the shape of the *L/V* interface is concave due to the intrinsic contact angle and the contact angle between the *L/V* that should be 180°. If the λ is larger than 254 μm, the shape changes from concave to convex. The details will be discussed later. It is clear that the three phase line consists of the *S/L/V* interfaces and the *L/V* interfaces and the shape is identical with that of Fig. 3c. On the other hand, the three phase line on a flat surface consists only of the *S/L/V* interface, as is well known.

3.2. Contact angles for loose lining round rod (LLRR) models

Figs 5 and 6 show the influence of the pitch on the contact angle for two kinds of aqueous solutions for the LLRR surfaces. The h_r value is 50 μm in Fig. 5 and 100 μm in Fig. 6.

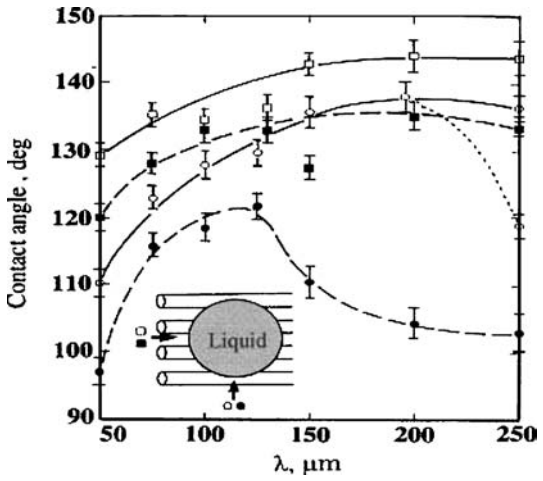

Figure 5 Influence of roughness pitch on contact angles for LLRR surface ($h_r = 50\ \mu$m). ○ and □: the pure water, ● and ■: the aqueous solution. □ and ■ : observed from parallel direction, ○ and ●: normal direction.

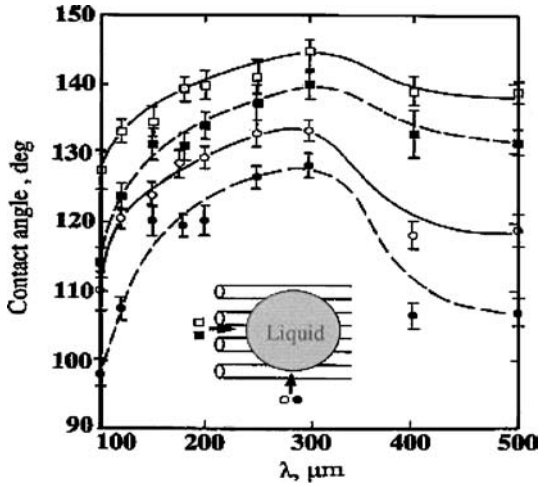

Figure 6 Influence of roughness pitch on contact angles for LLRR surface ($h_r = 100\ \mu$m).

The contact angle of pure water is greater than that of the one of the aqueous solution as expected due to the difference in the surface tension. The contact angle observed from the normal direction shows a maximum at the 125 μm pitch for the pure water system and at 200 μm for the aqueous solution as shown in Fig. 5. If we observe the contact angle from the normal direction, two contact angles are recognized in the case of the pure water system measured at the 250 μm pitch. If we summarize these results in a contact angle histogram, we can clearly confirm that there are two peaks. This suggests that the contact angle at the pitch of 200 μm should be the maximum contact angle and that of the 250 μm pitch is a critical value for touching and non-touching of the liquid drops to the substrate. Therefore, the contact angles are not constant and go through a maximum at the critical pitch for both solutions. These details will be discussed later.

The contact angles observed from the parallel direction are larger than those in the normal direction. These results are nearly identical with that of the 100 μm samples, nevertheless, the maximum contact angles are clearly observed at the pitch of 300 μm in all systems as shown in Fig. 6.

3.3. Contact angles for the loose packing sphere (LPS) models

Fig. 7 shows the influence of the roughness pitch on the contact angle for the two liquids using the ball bearings whose diameter was 200 μm, and using 300 μm diameter ball bearings in Fig. 8. These contact angles are changed with the pitch and go through a maximum at the 330 μm pitch for the 200 μm ball bearings and at 420 μm for the 300 μm ball bearings in both solutions. These results are nearly identical with those obtained for the LLRR surface. There are also two contact angles measured for the 300 μm ball bearings at the pitch of 598 μm for pure water. The explanation is given in Fig. 9. This means that there are two kinds of contact angle modes, namely touching and non-touching to the substrate, recognized in this case, and this phenomenon is identical with that observed for the LLRR surfaces as shown in Fig. 6.

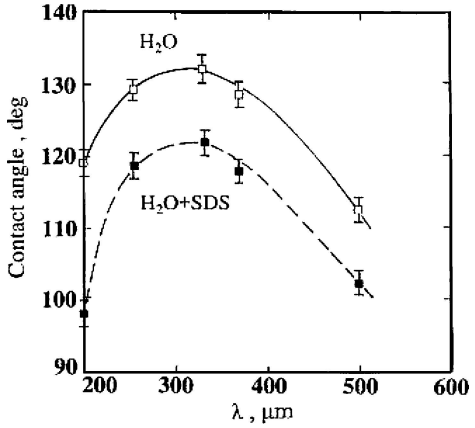

Figure 7 Influence of roughness pitch on contact angles for LPS surface ($h_r = 200\ \mu$m).

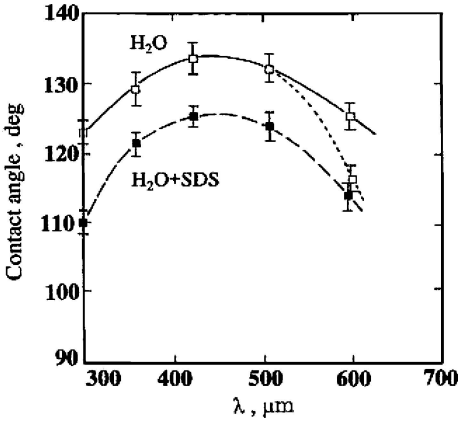

Figure 8 Influence of roughness pitch on contact angles for LPS surface ($h_r = 300\ \mu$m).

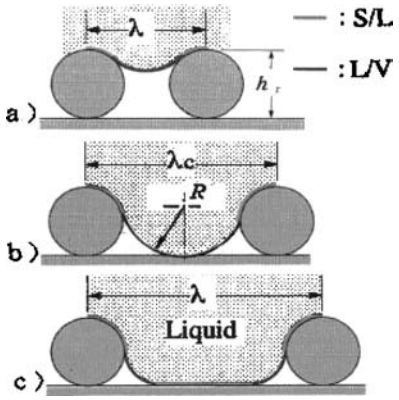

Figure 9 Wetting models of *S/L/V* interface for LPS models: (a) Model-1: $\lambda < \lambda_c$, (b) Model-2: $\lambda = \lambda_c$, (c) Model-3: $\lambda > \lambda_c$.

4. Discussion

4.1. Critical spacing

Figs 5 and 6 show the influence of the roughness pitch on the contact angle observed from the parallel and normal directions of the rods for a LLRR surface. The contact angle ϕ is not independent of the pitch, λ, and there are a critical pitch, λ_c, at which the contact angles show a maximum for both systems. This critical pitch, the longest pitch for the non-contact of a liquid drop at the substrate, should agree with the maximum contact angles. The λ_c is from 125 to 200 μm as shown in Fig. 5 and 300 μm in Fig. 6. The critical radius curvature of

the L/V interface at the S/L/V interface, R_c, should be more than half of λ_c. Therefore, these estimation values are nearly identical with our previous estimation, the radius curvature is 75 μm [7], namely their spacing is 150 μm.

If λ is less than λ_c, the bottom of the liquid drop does not touch the substrate as schematically shown in Fig. 9, then the contact angle increases with the pitch. The contact angles, observed from the normal direction, disperse widely from the advancing one to receding one, namely the hysteresis, when the spacing is less than the critical. These LLRR models' data, observed from the parallel direction, can then be treated with the model of Drelich *et al*. [6, 17] as the periphery of the liquid drop sits on the rod. However, the contact angles observed from the normal direction in Figs 5 and 6 are always the advancing ones because there is no barrier and the periphery sits not only on the rod but floats in the space. This contact angle can be discussed based on the Cassie equation [4]. Therefore, the contact angle observed from the parallel direction is greater than that of the normal one. Of course, we can discuss the contact angles observed from the normal direction by the identical method for the LPS models.

For example, for an increase in λ up to λ_c, the *L/V* interfacial area increases with the pitch to increase the contact angle. If the spacing becomes larger than λ_c, a part of the *L/V* interface changes into *S/L* interface as shown in Fig. 9c. If we look at the *S/L/V* interfacial line, three interfaces can be confirmed, namely, the ball $(S_b)/L$, substrate $(S_s)/L$ and *L/V* interfaces. Nevertheless, the S_b/L interface is identical with the S_s/L interface due to the paraffin coatings. We can then divide them into two interfaces, the paraffin/L and *L/V* interfaces. The interfacial morphology is essentially identical with that of Fig. 9c. Therefore, the apparent contact angle will decrease due to the touch as can be estimated using Equation 5, then the contact angle decreases with an increase in the pitch.

$$\cos\phi = r_{w1} f_1 \cos\theta_1 + r_{w2} f_2 \cos\theta_2 \tag{5}$$

We have already discussed the results of the close packing sphere and rod surfaces for non-wetting systems [7] using the Cassie equation [4]. The apparent contact angle, ϕ, can be expressed by Equation 5 using the roughness factor, r_w, the intrinsic contact angle, θ_1, for paraffin and θ_2 for the vapor. The θ_1 value is 107° and θ_2 should be 180°. At that time, we developed the hypothesis that the radius of curvature of the liquid at the *L/V* interface, R, is nearly constant and independent from the roughness height, $h_{r,}$ and that is more than 75 μm. In the model, f_1 is the projected area fraction of the *S/L* interface and f_2 is the projected area fraction of the *L/V* interface. Then, $(r_{w1} f_1 + r_{w2} f_2)$ equals 1.0 and f_2 increases with the decrease in h_r. Therefore, we have to rewrite the Cassie equation using each roughness factor r_{wi}, as Equation 5.

We have to consider the new interface model using the model shown in Fig. 9. At that time, for the calculation of the *L/V* interfacial area, $r_{w2} f_2$, we can make the estimation based on the radius of curvatures $R1$ and $R2$ for the LLRR model. The $R2$ must be much larger than that of the $R1$. Therefore, the ratio, $r_{w1} f_1 / r_{w2} f_2$ is then equal to the ratio, $h_r\ \phi / 2R1\ \phi$, and $r_{w1} f_1$ is $0.5\ h_r/(0.5\ h_r + R1)$ and $r_{w2} f_2$ is $R1/(0.5\ h_r + R1)$, then Equation 5 should be reconsidered. Therefore, if the roughness height, h_r, decreases to zero, then the contact angle, ϕ, increases to 180° like a small water drop on a lotus leaf because of the cosϕ value becomes −1.0. This estimation does not agree with our experimental results in Figs 5 and 6. We then calculated the R based on Fig. 5 using Equation 6. The model−2 in Fig. 9b can be also use for the explanation of R in the LPS surface due to the 2-dimentional isotropy.

$$\cos\phi = \frac{0.5\,h_r}{0.5\,h_r + R}\cos\theta_1 - \frac{R}{0.5\,h_r + R} \tag{6}$$

4.2. Curvature of liquid at *S/L/V* interface

The shape of the liquid drop is controlled by the Laplace equation [18]. If we assume that the radius of curvature at the *L/V* interface is almost axis-symmetry, we can then also calculate$R$ for the liquid surface at the *S/L* interface using Equations 7 and 8

$$\gamma_{LV}\left(\frac{1}{R_1} + \frac{1}{R_2}\right) = \frac{2\gamma_{LV}}{r_0} + gZ(\rho_L - \rho_V) \tag{7}$$

$$\frac{1}{R} = \frac{1}{r_0} + \frac{gZ(\rho_L - \rho_V)}{2\gamma_{LV}} \tag{8}$$

Assuming r_0: radius of the liquid drop = 1.0 mm for 4 ml, $R = R_1 = R_2$: radius of curvature at the L/V interface, Z: depth from the top to the substrate, ρ_L and ρ_V: specific density of the liquid and the vapor.

The R value is nearly 900 μm at $\phi = 115°$ for the LPS models and in the case of the LLRR models, R_2 should be infinite at the bottom, then R_1 becomes about 450 μm. Nevertheless, at the three phase line, $R_1 = R_2$ is much better than that of the R = infinite as can be seen in Fig. 3. These values also do not agree with our experimental results. We calculated the radius of curvature, R, for the *L/V* interface using the following Equation 9, introduced from Equation 6 based on the h_r and ϕ value.

$$\begin{aligned} R &= 0.5\,h_r \cdot \cos\theta_1 - (0.5\,h_r + R)\cos\phi \\ &= \frac{0.5\,h_r(\cos\theta_1 - \cos\phi)}{1 + \cos\phi} \\ &= \frac{0.5\,h_r(\cos 107° - \cos\phi)}{1 + \cos\phi} \end{aligned} \tag{9}$$

These results are shown in Fig. 10 for the pure water LLRR models ($h_r = 50$ μm and 100 μm) and Fig. 11 for the LPS models ($h_r = 200$ μm and 300 μm). The R values for the LPS models agree with our previous result [7].

We then have to correct the previous statement where R should be a function of h_r, θ_1 and γ_{LV}, and mainly

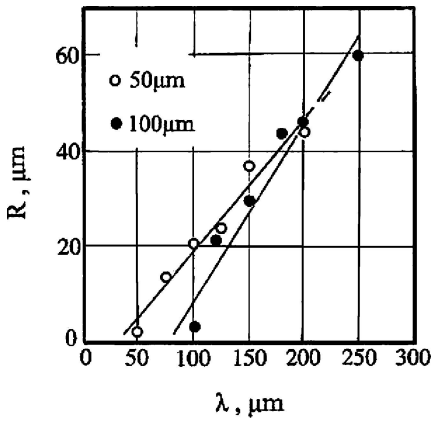

Figure 10 Calculated curvature of liquid surface at *S/L/V* interface for pure water LLRR surfaces.

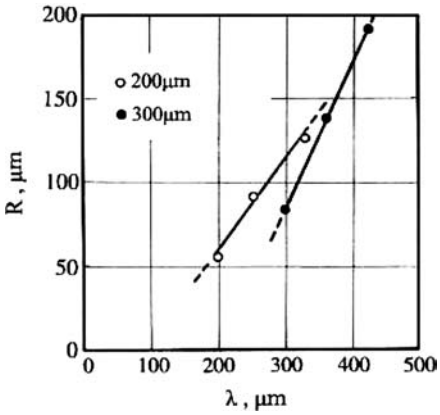

Figure 11 Calculated curvature of liquid surface at *S/L/V* interface for pure water LPS surfaces.

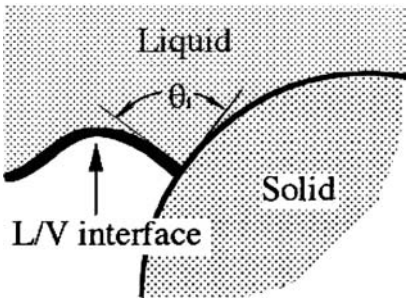

Figure 12 Schematic model of L/V interface at $S/L/V$ line.

controlled by the intrinsic contact angle, θ_1, at the *S/L/V* line, as shown in Fig. 12. Nevertheless, assuming that the entire shape of the *L/V* interface is independent from θ_1, the maximum value of the R should be controlled by the Laplace equation [18], then R can converge to the R calculated using the Laplace equation. Therefore, R can be expressed as follows using the Johnson-Mehl's equation:

$$R = A\{1 - \exp(-Bh_r)\} \tag{10}$$

in which, A is a function of θ_1 and γ_{LV}, and B is constant.

If we look at Fig. 11, R is greater than 50 μm when λ is greater than h_r. This means that the relationship between R and λ can be simply expressed by a linear functional equation. When h_rs are 200 μm and 300 μm

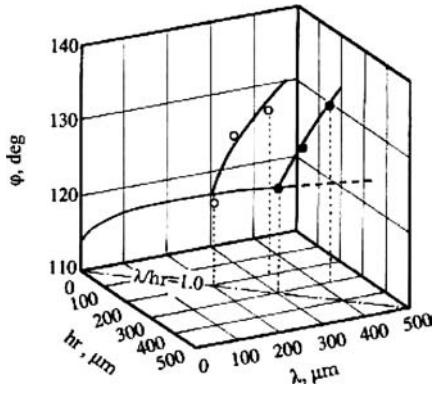

Figure 13 Influence of roughness pitch and roughness height on contact angle, ϕ, for pure water LPS surfaces.

for the LPS models, R is expressed as follows.

$$R_{200} = 0.55\,\lambda - 51 \quad \text{and} \quad R_{300} = 0.88\,\lambda - 180 \tag{11}$$

If we calculate the contact angle, ϕ, for the pure water LPS models based on R, using Equation 6 along with R_{200}, R_{300} and λ. These results are shown in Fig. 13. These results show that R is from about 50 μm to 200 μm. As can be seen clearly, R increases with the λ. This is the main reason why the contact angle increases with the pitch. These figures are in good agreement with our previous estimation values and with our experimental results.

Nevertheless, there is another problem for the contact angles. There are microscopic (local) contact angles and macroscopic contact angles in one liquid drop. This result is identical with our previous study [17]. This means that the Young local contact angle is the boundary condition of the Laplace equation the, the macroscopic both contact angles for the LLRR surfaces are controlled by the interfacial energy to decrease the total energy to a minimum. Therefore, we cannot precisely discuss the both macroscopic contact angles due to the high anisotropy of the model surfaces. If the model is isotropic, we can use the identical model as the idealized rough surface by Johnson and Dettre [19] only for the contact angle observed from the normal direction. However, their model is too simplified. Therefore the results of the LPS model can be discussed using our new model such as Equation 6.

5. Conclusions

The effect of surface roughness on the wettability in non-wetting systems has been investigated using two kinds of surface model, a loose packing of sphere model and a loose lining of round rod model. We independently discussed the influence of the roughness height and roughness pitch on wettability using the sessile drop method for a paraffin/aqueous solutions. The experimental results show that the apparent contact angles go through a maximum at the critical pitch for both systems. This means that there is an appropriate pitch which shows the maximum contact angle. The pitch should be determined by the surface tension of

the liquid, the contact angle, the roughness height (the diameter of ball and rod).

If the roughness pitch is less than a critical value, the apparent contact angle increases with the pitch, and if the roughness pitch is greater than the critical value, the apparent contact angle decreases with the pitch due to the touch of the drop at the substrate. These results can be explained by the ratio of the solid/liquid and liquid/vapor line length at the three phase line.

References

1. R. N. WENZEL, *Industr. Eng. Chem.* **28** (1936) 988.
2. R. SHUTTLEWORTH and G. L. BAILEY, *Discuss. Farady Soc.* **3** (1948) 16.
3. R. E. JOHNSON, JR. and R. H. DETTRE, *Surf. Colloid Sci.* **2** (1969) 85.
4. A. B. D. CASSIE and S. BAXTER, *Trans. Faraday Soc.* **40** (1944) 546.
5. A. B. D. CASSIE, *Discuss. Fraday Soc.* **3** (1948) 11.
6. J. DRELICH, J. L. WILBUR, J. D. MILLER and G. M. WHITESIDES, *Langmuir* **12** (1996) 1913.
7. H. NAKAE, R. INUI, Y. HIRATA and H. SAITO, *Acta Mater* **46** (1998) 2313.
8. J. DRELICH, J. D. MILLER, A. KUMAR and G. M. WHITESIDES, *Colloids Surf. A: Physicochemi. Engng. Asp.* **93** (1994) 1.
9. J. DRELICH and J. D. MILLER, *Langumuir* **9** (1993) 619.
10. N. MORI, M. UKITA and K. OHGI, *J. Japan Inst. Metals.* **55** (1991) 820.
11. S. J. HITCHCOCK, N. T. CARROLL and M. G. NICHOLAS, *J. Mater. Sci.* **16** (1981) 714.
12. A. KAWAI and H. NAGATA, *Jpn. J. Appl. Phys.* **33** (1994) Pt.2, No.9A, L1283.
13. X. B. ZHOU and TH. M. DE HOSSON, *J. Mater. Res.* **10** (1995) 1984.
14. F. E. BARTELL and J. W. SHEPARD, *J. Phys. Chem.* **57** (1953) 211, 455, 458.
15. S. ASAHARA and K. GOTO, *KOGYOKAGAKU* **58** (1955) 864.
16. G. NAVASCUES, *Rep. Prog. Phys.* **42** (1979) 1131.
17. H. FUJII, H. NAKAE and K. OKADA, *Acta Metall. Mater.* **41** (1993) 2963.
18. Physical Chemistry of Surfaces, 4th ed., edited by A. W. Adamson (John Willey & Sons, 1982) p. 7.
19. R. E. JOHNSON, JR. and R. H. DETTRE, Contact Angle, Wettability, and Adhesion, Advances in Chemistry Series 43, American Chemical Soc. (1964) p. 112.

Received 31 March
and accepted 18 July 2004